Journal for ImmunoTherapy of Cancer

Generation of a safe and efficacious llama single-domain antibody fragment (vHH) targeting the membrane-proximal region of 4-1BB for engineering therapeutic bispecific antibodies for cancer

Tianhang Zhai ,[1] Chao Wang,[2] Yifeng Xu,[3] Weifeng Huang,[3] Zhijun Yuan,[2] Tao Wang,[2] Shuang Dai,[3] Shaogang Peng,[3] Tuling Pang,[2] Wenchao Jiang,[2] Yuhua Huang,[2] Yuefeng Zou,[2] Yingda Xu,[2] Joanne Sun,[2] Xinjiang Gong,[2] Jinping Zhang,[4] Andy Tsun,[2] Bin Li,[1] Xiaoniu Miao[2,4]

To cite: Zhai T, Wang C, Xu Y, *et al*. Generation of a safe and efficacious llama single-domain antibody fragment (vHH) targeting the membrane-proximal region of 4-1BB for engineering therapeutic bispecific antibodies for cancer. *Journal for ImmunoTherapy of Cancer* 2021;**9**:e002131. doi:10.1136/jitc-2020-002131

► Additional supplemental material is published online only. To view, please visit the journal online (http://dx.doi.org/10.1136/jitc-2020-002131).

TZ and CW are joint first authors.

Accepted 23 May 2021

For numbered affiliations see end of article.

Correspondence to
Dr Xiaoniu Miao;
miao.xn@biotheus.com

Professor Bin Li;
binli@shsmu.edu.cn

Dr Andy Tsun;
tsun.a@biotheus.com

ABSTRACT

Background The discovery of checkpoint inhibitors towards cytotoxic T-lymphocyte protein 4 (CTLA-4) and programmed cell death protein 1 (PD-1) has been revolutionary for the treatment of cancers. These therapies have only offered an average of 20%–30% response rates across the tumor spectrum and the combination of agonists towards the tumor-necrosis superfamily members, such as 4-1BB and CD40, has shown potent efficacy in preclinical studies; however, these agonists have exhibited high degrees of toxicity with limited efficacy in human trials. In this study, we have generated a single-domain antibody towards a unique epitope of 4-1BB that limits its potential on-target toxicity while maintaining sufficient potency. This 4-1BB binder is ideal for use in the engineering of multispecific antibodies to localize 4-1BB activation within the tumor microenvironment, as shown here by a anti-PD-L1/4-1BB bispecific candidate (PM1003).

Methods To determine the functional activity of the 4-1BB- and PD-L1-binding elements of PM1003, *in vitro* luciferase reporter and primary cell assays were used to test the potency of programmed cell death 1 ligand 1 (PD-L1) blockade and PD-L1-mediated 4-1BB activation via cross-bridging. X-ray crystallography was conducted to resolve the binding epitopes of the respective binding arms, and accurate binding kinetics were determined using standard affinity measurement techniques. Human 4-1BB and/or PD-L1 knock-in mice were used in cancer models for testing the *in vivo* antitumor efficacy of PM1003, and safety was evaluated further.

Results PM1003 shows potent activation of 4-1BB and blockade of PD-L1 in cell-based assays. 4-1BB activation was exerted through the bridging of PD-L1 on target cells and 4-1BB on effector cells. No PD-L1-independent activation of 4-1BB was observed. Through X-ray crystallography, a unique binding epitope in the cysteine-rich domain 4 (CRD4) region was resolved that provides high potency and potentially low on-target toxicity as determined by primary immune cell assays and toxicity evaluation *in vivo*.

Conclusions A unique single-domain antibody was discovered that binds to the CRD4 domain of 4-1BB. When incorporated into a 4-1BB/PD-L1 bispecific (PM1003), we have shown the potent inhibition of PD-L1 activity with 4-1BB agonism upon cross-bridging with PD-L1 *in vitro*. Antitumor activity with minimal toxicity was found *in vivo*. Thus, PM1003 is a uniquely differentiating and next generation therapeutic agent for cancer therapy.

INTRODUCTION

The ultimate goal for the immunotherapy of cancer is to activate immune responses towards and kill tumor cells. Although these immune reactions often require the induction of inflammatory responses, these activation signals must be restrained to limit excess inflammation. A certain class of 'checkpoint' molecules mediate this process in a spatial and temporal manner.[1] Although the CTLA-4 and PD-1/PD-L1 class of inhibitors spurred this revolution in cancer therapy by conducting the so-called 'releasing of the brake' on the immune system, a large number of patients still do not respond, and early combination strategies with chemotherapies have tried to raise the survival rate of cancer patients.[2–5] Thus, the combination of these checkpoint inhibitors[6] and the investigation/identification of the biological mechanisms that determine whether a patient may respond to these therapies[7–9] was and still is of utmost importance.

Lymphocytes express costimulatory receptors that, when activated, can improve effector and memory responses. As such, the tumor necrosis

factor receptor superfamily of receptors (TNFRSF), which includes CD27, 4-1BB (CD137), OX40 (CD134) and GITR (CD357) have been targeted using agonist antibodies.[10] 4-1BB is a potent stimulator of T cells and natural killer (NK) cells and when activated in combination with checkpoint inhibitors may improve anticancer immune responses, especially in immunogenic-poor tumors.[11] Unfortunately, inherent on-target-related hepatotoxicity has been observed during the clinical development of Urelumab.[12 13] The next wave of discovery campaigns for 4-1BB agonists has been launched to address this issue by targeting different epitopes, optimizing binding affinities and through engineering different modes of Fc-mediated crosslinking.[14–16]

Most TNFR-superfamily members, such as 4-1BB, consist of four cysteine-rich domains (CRDs). The current understanding is that agonism towards TNFR-superfamily members (modeled on CD40) is strongest when antibodies bind to CRD1 (membrane distal) and weakest at CRD4 (membrane proximal).[17] Interestingly, Urelumab binds to CRD1 of 4-1BB and has shown potent agonist activity yet induces high liver toxicity, whereas Utomilumab, which binds between CRD3 and CRD4, has shown relative safety but with limited activity towards 4-1BB.[18] There is a concern that monospecific agonist antibodies may only offer a linear correlation between potency and toxicity. One strategy to reduce their liver-related on-target effects has been to optimize FcγR binding to FcγRs that are normally enriched in tumors,[16] but next-generation bispecific antibodies have an advantage through crosslinking 4-1BB receptors only in the presence of tumor-associated antigens (TAAs) through cross-bridging, and various programs are currently entering the clinic targeting TAAs such as epidermal growth factor receptor (EGFR) and human epidermal growth factor receptor 2 (HER2).[19–22]

PD-L1 (CD274, B7-H1), one of the ligands for PD-1, is a checkpoint regulator that restrains T cell activation during antigen presentation and effector function. PD-L1 expression has been identified in a wide variety of solid tumors, which makes it a potential TAA for PD-L1/4-1BB bispecific antibody development. In preclinical studies, significant synergistic effects have been observed when antibodies targeting both of these pathways are combined. PD-L1/4-1BB bispecific antibodies could therefore combine PD-L1 blockade and 4-1BB agonism to provide a substantial survival benefit in multiple mouse tumor models with low/no toxicity.[22]

Here, we report the discovery and development of a bispecific antibody towards PD-L1 and 4-1BB (PM1003). PM1003 potently blocks the interaction between PD-1 and PD-L1 and binds to 4-1BB at the CRD4 domain allowing for effective dose-dependent activation of 4-1BB in the presence of PD-L1, with minimal toxicity. The unique 4-1BB binding epitope has potential for hitting a sweet spot between efficacy and toxicity and we believe this discovery has resulted in the generation of a valuable 4-1BB agonist for creating more effective and safer 4-1BB-based multispecific therapeutics for cancer.

METHODS

Mice

Human PD-L1/PD-1/4-1BB triple knock-in mice were purchased from Gempharmatech (Jiangsu, China). Human PD-L1/4-1BB double knock-in mice and human 4-1BB knock-in mice were purchased from Biocytogen (Beijing, China). All mice were maintained under specified pathogen-free conditions, and all studies were approved by the Animal Care and Use Committee of HUST-Suzhou Institute for Brainsmatics.

Cells and cell lines

CT-26 and MC-38 cells knocked-in with human PD-L1 (CT-26-huPD-L1 and MC-38-huPD-L1 cells, respectively) were obtained from Gempharmatech (Jiangsu, China). Chinese hamster ovary (CHO) cells were obtained from Life technologies. Human PD-L1 (CHO-huPD-L1) and 4-1BB (CHO-hu4-1BB) overexpressing CHO cells were generated by the transduction of CHO cells with full length human coding sequences. 4-1BB-NF-κB luciferase reporter cells (Jurkat-hu4-1BB-Luc) were generated by the transduction of Jurkat cells (ATCC) with lentivirus from a NF-κB luciferase reporter plasmid (Promega) and a human 4-1BB-encoding vector.

Antibodies

The sequences of Urelumab and Utomilumab were obtained from patents US8137667B2 and US2012/0237498A1, respectively. Heavy and light chain genes were cloned into mammalian expression vector pcDNA3.1, expressed using the ExpiCHO system (Invitrogen) and protein was purified by protein A chromatography (GE).

Alpaca immunization and library construction

Alpacas were immunized subcutaneously with approximately 500 µg recombinant human PD-L1 (ACRO Biosystems) or 4-1BB protein (ACRO Biosystems) on days 0, 14, 28 and 42 with Freund's adjuvant (Sigma). Blood was collected 7 days after the final immunization to isolate peripheral blood mononuclear cell (PBMC). RNA was isolated using TRIZOL reagent (Life technologies). cDNA was synthesized using the SuperScript IV First-Strand Synthesis kit (Life technologies) primed with oligo (dT) and subsequently used to amplify the single domain antibody (vHH) repertoire. vHH libraries were constructed by cotransforming linearized pFabVH vector and the PCR product containing homology arms by yeast gap-repair. The pFab vector system allows the display of fusion proteins containing a vHH followed by Aga2p and a Myc tag (online supplemental figure 1A).

Selection of vHH by yeast display

Expression of vHH on the yeast cell surface was induced by culturing in G/RCAA (substituting 2 g/L galactose and raffinose for the dextrose in the SDCAA medium), and expression-positive yeast cells were sorted by magnetic bead aided cell sorting (Miltenyi) then 4× by fluorescence activated cell sorting (FACS) (BD, Aria III) using

biotinylated antigens). Individual clones were picked for sequencing.

Protein expression and purification

The DNA sequences for PD-L1 (19–134) was synthesized with a C-terminal 6x His-tag fusion and cloned into the pET21b vector for expression in *E. coli*. Protein was purified on a Ni-NTA column and then polished through a Superdex 75 Increase 10/300 GL Sciences (GL) column. The vHH HZ-C-Ye-18 was fused to human g1-Fc (HZ-C-Ye-18-Fc) in a pcDNA3.1 vector. The ExpiCHO expression system (Life technologies) was used to express the vHH-Fc antibodies according to the manufacturer's instructions. Cell culture was collected 5 days after transfection and purified by a Protein A column. The eluted protein was concentrated and first cleaved by IdeS. The resulting mixture was passed through Protein G columns to remove Fc, and then digested by GingisKHAN to generate HZ-C-Ye-18. 4-1BB (25-162) and HZ-L-Yr-16 were individually constructed by similar approaches as HZ-C-Ye-18. However, a truncated Fc with only Leu-Gly-Gly in the hinge region was cloned into the vector.[23] The encoded plasmid was transiently transfected into Expi293 cells (Life technologies) using polyethylenimine (PEI). For 4-1BB, the eluted protein was concentrated, cleaved by IdeS and purified by a Protein A column. The 4-1BB monomer was separated from 4-1BB homodimer using on a Superdex 75 Increase 10/300 GL column. For HZ-L-Yr-16, only one step purification was performed using a Protein G column after IdeS cleavage.

Crystallization, X-ray data collection and structure determination

vHH and antigen were mixed in a 1:1 molar ratio and purified on a Superdex 75 Increase 10/300 GL column. Crystals were grown in 96-well plates by sitting drop vapor diffusion (protein:buffer:reservoir of 0.4 µL:0.4 µL:40 µL). The PD-L1:HZ-C-Ye-18 complex and 4-1BB:HZ-L-Yr-16 complex were crystallized in 0.2 M $(NH_4)_2SO_4$, 0.1 M Bis-Tris pH 5.5, 25% w/v PEG 3350 and 1.5 M Li_2SO_4, 100 mM Tris pH 8.5, 10 mM $NiSO_4$, respectively. For data collection, the crystals were soaked in a reservoir solution containing 20% (v/v) glycerol and flash-frozen in liquid nitrogen (Viva Biotech (Shanghai) Limited).

Diffraction images were collected at the Shanghai Synchrotron Radiation Facility beamline BL19U1 (for PD-L1:HZ-C-Ye-18) and BL18U1 (for 4-1BB:HZ-L-Yr-16) on a Pilatus detector and were indexed, integrated and scaled using XDS.[6] Resolution limits were cut off at $I/\sigma(I)=2.2$ and 3.1 for PD-L1:HZ-C-Ye-18 and 4-1BB:HZ-L-Yr-16 complex, respectively.[24] Phases were determined by molecular replacement with Phaser[25] using the PD-L1 structure (PDB: 5JDS) and the vHH structure (PDB: 5M2J) for the PD-L1:HZ-C-Ye-18 complex, 4-1BB structure (PDB: 6MGP) and the vHH structure (PDB: 4XTA) for 4-1BB:HZ-L-Yr-16 complex as search models. Structure refinement was carried out using Refmac5.[26] Model inspection, manual rebuilding and structure validation was performed using crystallographic object-oriented toolkit (COOT).[27] Figures and structural alignments and superpositions were generated using PyMOL.

Cell binding assay

CHO-hu4-1BB or CHO-huPD-L1 cells were incubated for 30 min with a series dilution of antibodies. After washing, the cells were incubated with phycoerythrin (PE)-goat (ab')2 antihuman Fc antibody (abcam) for 30 min at 4°C. Stained cells were analyzed on a CytoFlex system (Beckman). Median fluorescent intensity values were plotted against the concentration of primary antibody.

Cell based blocking assay

Antibodies were incubated with CHO-hu4-1BB cells for 30 min, followed by incubation with biotinylated human 4-1BB ligand (ACROBiosystems) for 30 min at room temperature. The cells were washed and subsequently incubated with Streptavidin, R-Phycoerythrin Conjugate (SA-PE) (ThermoFisher) at 4°C for 20 min. Fluorescence signals were determined on a CytoFlex system and results were analyzed using GraphPad7 software.

Biotinylated human PD-L1 (ACROBiosystems) was incubated with a concentration gradient of antibodies for 30 min. The mixtures were added to CHO-huPD-1 cells and incubated for 1 hour at 4°C. The cells were then stained with SA-PE for 20 min. The fluorescence signals were determined on a CytoFlex system and results were analyzed using GraphPad Prism software.

Production of a 4-1BB/PD-L1 bispecific antibody PM1003

A PD-L1/4-1BB bispecific antibody named PM1003 was generated by fusing the anti-4-1BB vHH to the C terminus of anti-PD-L1 vHH-Fc through a 20-residue-long linker. PM1003 incorporates LALA mutations (leucine to alanine at positions 234 and 235 according to Eu numbering) in the CH2 domain to reduce Fc receptor binding.[28 29] PM1003 was expressed transiently using HEK293F cells (Invitrogen). Supernatants were purified on MabSelect SuRe LX Protein-A prepacked columns on an ÄKTAxpress instrument (GE Healthcare Life Sciences).

Cell bridging

CHO-huPD-L1 cells were stained with Cell Trace CFSE (ThermoFisher), while CHO-hu4-1BB cells were stained with CellTracker Deep violet (ThermoFisher) following the manufacturer's standard methodology. After staining, cells were washed and resuspended. Labeled cells were mixed and incubated for 2 hours at 37°C with titrated antibodies. After incubation, samples were evaluated on a CytoFlex system. Data were plotted using GraphPad Prism Software.

Binding ELISA

Human 4-1BB, GITR, OX40 or CD40 (ACRO Biosystems) were coated onto a 96-well plate overnight at 4°C. The plate was washed and blocked for 1 hour in 5% bovine serum albumin/phosphate buffered saline (BSA/PBS) at room temperature. Serially diluted antibodies were added to the plate in duplicate and incubated for 1 hour at room

temperature. After washing, Goat (ab')2 antihuman IgG Fc (HRP) (Abcam) was added and incubated at room temperature for 1 hour. Plates were washed and signal developed using 3,3',5,5'-tetra-methylbenzidine substrate solution (Solarbio) according to manufacturer's instructions. Absorbance at 450 nm was read on a Molecular Devices SpectraMax i3 system with SoftMax Pro software.

Co-binding ELISA

Human 4-1BB protein was coated onto a 96-well plate overnight at 4°C. After washing and blocking, serially diluted antibodies were added to the plate and incubated for 1 hour at room temperature. After washing, biotinylated human PD-L1 protein (KACTUS) was added and incubated at room temperature for 1 hour. Plates were washed and the signal was developed using streptavidin (HRP) (Abcam) according to manufacturer's instructions.

Primary T cell activation assay

Human primary T cells were isolated from frozen PBMC (SAILYBIO) using the human total T cell isolation kit (STEMCELL) according to the manufacturer's instructions. Anti-CD3 antibody, OKT-3 (Biolegend), was coated (1 µg/mL) on NUNC flat-bottom plates (ThermoFisher) for 2 hours at 37°C then washed twice with PBS. Serially diluted anti-4-1BB antibodies or control antibodies were either coated after OKT-3 for 2 hours followed by washing or added to the culture medium and incubated with human primary T cells for 4 or 5 days. Cell supernatants were measured for secreted IFN-γ levels by ELISA (eBioscience). PD-L1 negative or PD-L1 positive CHO cells were co-cultured with human primary T cells in X-VIVO15 medium (LONZA) in the presence of plate bound 1 µg/mL OKT3 and serially diluted test antibodies for 2 days at 37°C. After incubation, cell supernatants were measured for secreted IL-2 levels by ELISA (eBioscience).

Mixed lymphocyte reaction (MLR) assay

Monocytes were isolated from PBMC. Monocyte-derived dendritic cells (moDCs) were generated by culturing the monocytes in X-VIVO15 medium with 10 ng/mL GM-CSF and 20 ng/mL IL-4 (R&D Systems) for 6 days. Human primary T cells were isolated from a different PBMC donor source and then cocultured with the moDCs in a 96-well plate and serially diluted antibodies for 3 days. Cell supernatants were measured for secreted IL-2 levels by ELISA (eBioscience).

NF-κB luciferase reporter assay

PD-L1-negative or PD-L1-positive CHO cells were co-cultured with Jurkat-hu4-1BB-NF-κB-Luc cells in the presence of 1 µg/mL OKT-3 and serially diluted antibodies for 16 hours at 37°C. Bio-Glo Reagent (Promega), prepared according to manufacturer's instructions, was added and fluorescence measured using a SpectraMax i3 system with SoftMax Pro software (Molecular Devices).

In vivo efficacy studies

Human PD-L1/PD-1/4-1BB triple knock-in BALB/c mice aged 8–10 weeks each received 1×10^6 CT-26-huPD-L1 cells injected subcutaneously in the left flank. Tumor volume measurements were taken with calipers to determine the longest and shortest axes of the tumor and the following formula was used to calculate tumor volume: 'tumor volume (mm^3)=Length×Width^2/2'. Dosing was initiated when tumors were an average of 100 mm^3. Antibodies were injected intraperitoneally into mice on days 7, 9 and 11.

Hepatotoxicity measurement

To study the hepatotoxic effects of our samples, human 4-1BB knock-in mice were treated with 10 mg/kg Urelumab or 6.67 mg/kg PM1003 i.p. every 5 days for four doses in total. Seven days after the final dose, alanine aminotransferase (ALT) levels in the blood were analyzed using the Alanine Transaminase Activity Assay Kit (abcam) following the manufacturer's instructions. Liver pathology was assessed by H&E and immunohistochemistry (IHC) staining by Servicebio (Wuhan, China).

RESULTS

Discovery of a 4-1BB-specific vHH with agonist activity

To generate vHHs specifically recognizing 4-1BB, alpacas were immunized with recombinant human 4-1BB protein and a yeast display library was generated. The library was screened against both human and cynomolgus (cyno) 4-1BB to identify human and cyno cross-reactive vHH sequences with a broad range of binding affinities and epitope coverage. In mind of potential efficacy versus safety issues, clone L-Yr-16 was chosen for humanization (HZ-L-Yr-16) due to its mild agonist activity, and fused to a human g1-Fc containing LALA mutations (online supplemental figure 1B) to remove Fc effector function (HZ-L-Yr-16-Fc).

HZ-L-Yr-16-Fc binds to both human and cyno 4-1BB-overexpressing CHO cells in a dose-dependent manner (figure 1A,B), whereas Urelumab only bound to human 4-1BB-expressing cells due to the lack of cyno 4-1BB cross-reactivity. ELISA-based binding data revealed that HZ-L-Yr-16-Fc binds strongly to human 4-1BB, but not to any other TNFR-superfamily members (figure 1C). A cell-based blocking assay was used to show that HZ-L-Yr-16-Fc is a ligand non-blocker, while Utomilumab is a blocker and Urelumab is a partial blocker (figure 1D).

To demonstrate that HZ-L-Yr-16-Fc can induce human 4-1BB signaling, activated human primary T cells (by plate-bound OKT3), were cocultured with anti-4-1BB antibody either plate-bound or in solution. Both plate-bound HZ-L-Yr-16-Fc and Urelumab showed T cell stimulation activity as measured by IFN-γ release, while Utomilumab showed the weakest agonism in the assay (figure 1E). HZ-L-Yr-16-Fc did not show any stimulation in solution phase, indicating that

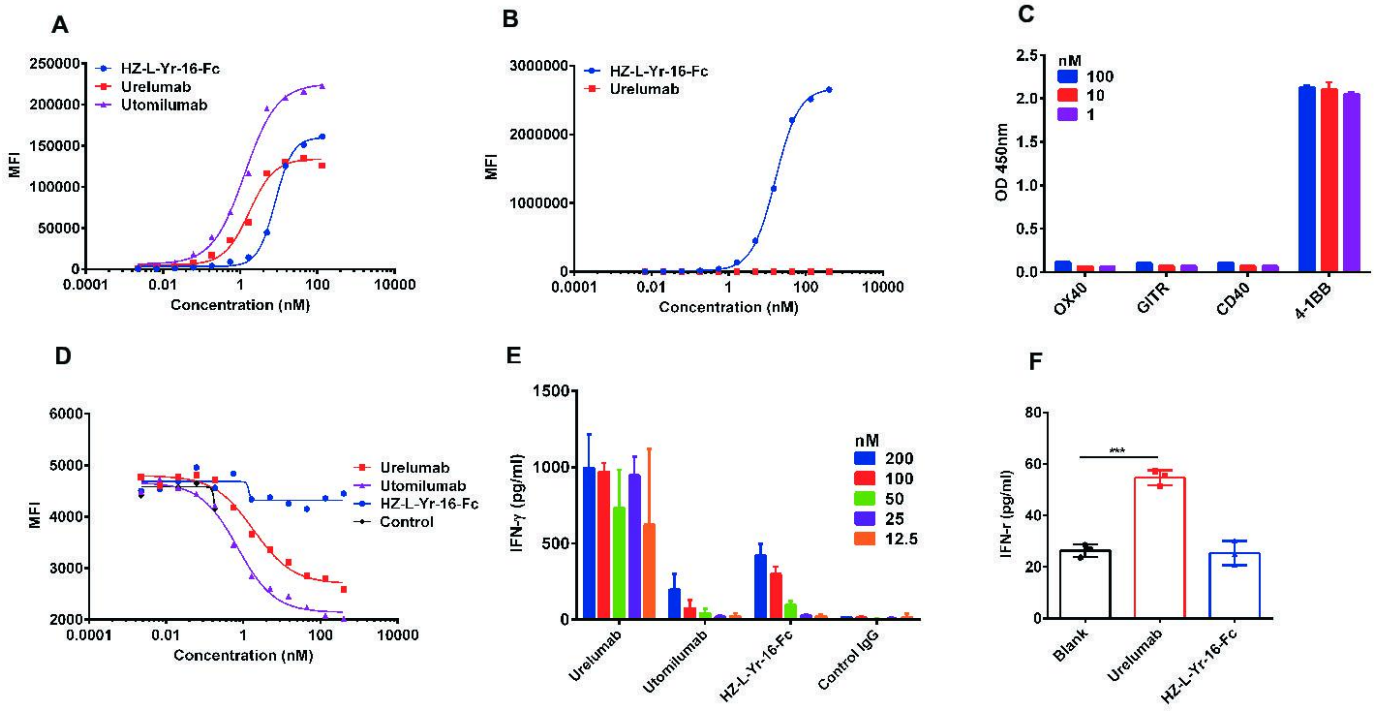

Figure 1 Characterization of anti-4-1BB antibody (HZ-L-Yr-16-Fc). Binding activity of HZ-L-Yr-16-Fc to human 4-1BB (A) or cyno 4-1BB (B) overexpressing CHO cells as revealed by flow cytometry analysis. (C) Binding of HZ-L-Yr-16-Fc to OX40, GITR, CD40, 4-1BB determined by ELISA. (D) Effect of indicated anti-4-1BB antibodies blocking 4-1BB ligand binding to 4-1BB measured by flow cytometry. (E) Purified T cells from human PBMC were stimulated with plated anti-CD3 and indicated anti-4-1BB antibodies. Five days later, IFN-γ in the culture medium was analyzed by ELISA. (F) Purified T cells from human PBMC were stimulated with plated anti-CD3 and indicated anti-4-1BB or anti-CD28 antibodies in solution. Five days later, IFN-γ in the culture medium was analyzed by ELISA. Data are mean±SD, ***p<0.001.

crosslinking is required for HZ-L-Yr-16-Fc-mediated agonism. However, Urelumab could stimulate T cells when added into the solution phase without crosslinking (figure 1F). These data indicate that HZ-L-Yr-16-Fc has a different binding and agonism profile compared with Urelumab and Utomilumab.

Structural determination of the 4-1BB:anti-4-1BB vHH complex

Based on the unique functional traits of HZ-L-Yr-16-Fc, we sought to understand better its binding profile towards 4-1BB by X-ray crystallography. HZ-L-Yr-16 was found to interact with 4-1BB at a unique epitope located at the membrane-proximal CRD4 region of 4-1BB (figure 2A). The primary interaction sites of HZ-L-Yr-16 with 4-1BB are located in the CDR2 and CDR3 regions of the vHH. The CDR2 and CDR3 loops form hydrogen bonds with residues D142, R154, V156, C158 and G159 of 4-1BB (figure 2B, online supplemental table 1). Additionally, HZ-L-Yr-16 grips the two β-strands of CRD4 at the hydrophobic pocket formed by the residues V32, A33, Y37, L47, I52, Y97, Y102, Y112 and W115 (online supplemental figure 2A). The binding interface is also mediated by salt bridges between R154 of 4-1BB and D55 or D57 of HZ-L-Yr-16 (online supplemental figure 2B).

Urelumab (PDB: 6MHR) binds to the N-terminus of 4-1BB (CRD1), whereas Utomilumab (PDB: 6MI2) interacts with the domain 3–4 junction.[18] HZ-L-Yr-16 binds to the membrane-proximal region and does not appear to interfere with ligand engagement (figure 2C). These differences in binding were consistent with our competitive epitope binning data which shows that HZ-L-Yr-16 does not compete with Urelumab and Utomilumab for binding to 4-1BB (online supplemental figure 3). Interestingly, on binding to ligand or the different antibodies, 4-1BB shows conformational changes by bending between the A2 and A1 motifs of CRD3 (online supplemental figure 2C).

Discovery of a PD-L1-specific vHH with potent PD-L1 blocking activity

Alpacas were immunized with recombinant human PD-L1 protein, followed by vHH selection by yeast display. Clone C-Ye-18 was selected as the final lead, which binds specifically to PD-L1 with an estimated affinity in the low nM range. C-Ye-18 was humanized and fused to a human g1-Fc (HZ-C-Ye-18-Fc) with its Fc effector function silenced (LALA). *In vitro* cell-based binding and blocking experiments indicated that HZ-C-Ye-18-Fc could bind to cell surface PD-L1 and competes with PD-1 for PD-L1, with a potency similar to that of Atezolizumab (online supplemental figure 4A,B). *In vivo* efficacy experiments indicated that HZ-C-Ye-18-Fc can effectively control tumor growth in a hPD-L1 knock-in tumor mouse model (online supplemental figure 4C).

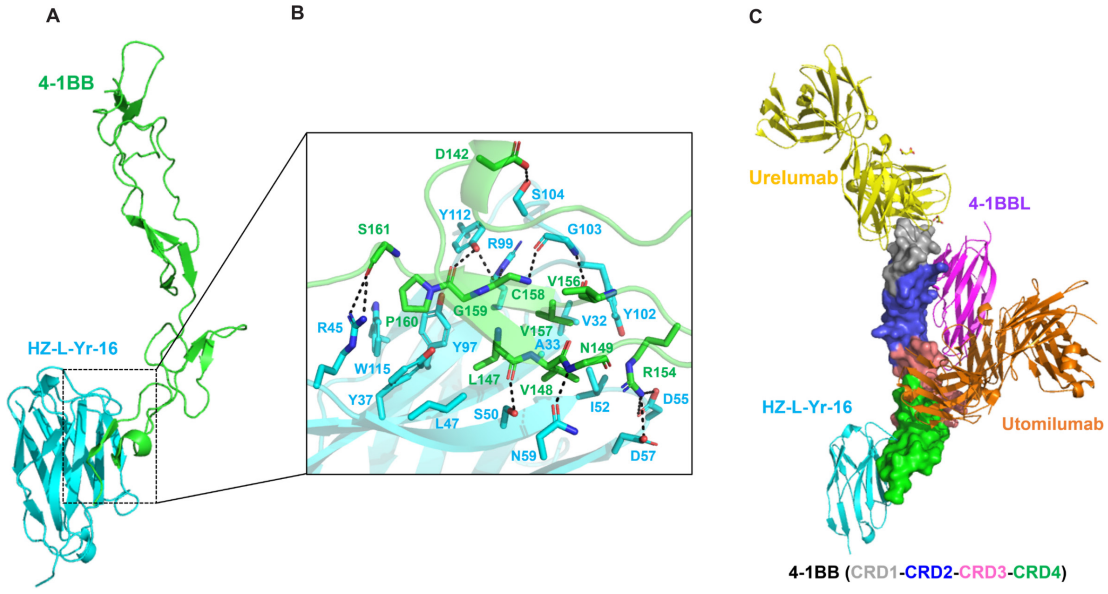

Figure 2 Detailed interaction sites between the 4-1BB and HZ-L-Yr-16 and epitope comparison between different antibody agonists. (A) Overall structure of the 4-1BB: HZ-L-Yr-16 complex. 4-1BB is shown in green; HZ-L-Yr-16 is shown in cyan. (B) The interactions between 4-1BB and HZ-L-Yr-16. Hydrogen bonds are shown as black dashed lines. (C) Epitope comparison of HZ-L-Yr-16 (in cyan), Urelumab (yellow) and Utomilumab (orange). 4-1BBL (in magenta) is also aligned for comparison.

Structural determination of the PD-L1:anti-PD-L1 vHH complex

To investigate the binding epitope of our anti-PD-L1 vHH the structure of the PD-L1:HZ-C-Ye-18 complex was resolved to a 1.64Å resolution. The overall structure of the PD-L1:HZ-C-Ye-18 complex is shown in figure 3A. Analysis of the PD-L1:HZ-C-Ye-18 binding interface with proteins, interfaces, structures and assemblies (PISA) shows how each protein buries within a ~838Å^2 surface area. All three CDRs of HZ-C-Ye-18 contain contact residues with PD-L1 through a number of hydrogen bonds and hydrophobic interactions (figure 3B). The CDR1, CDR2 and CDR3 loops were observed to form hydrogen bonds with the residues Y56, N63, H69, D73, K75, S117 and G119 of PD-L1. Additionally, Y32, W33 and Y35 from the highly hydrophobic CDR1 are involved in the hydrophobic interface between HZ-C-Ye-18 and PD-L1, as well as Y59 from CDR2 and P100/Y103 from CDR3. The binding epitope for HZ-C-Ye-18 shows similarity with FDA-approved PD-L1 antibodies, including Atezolizumab (PDB: 5X8L),[30] Avelumab (PDB: 5GRJ)[31] and Durvalumab (PDB: 5X8M)[30] (online supplemental figure 5A). The low contact area did not affect its *in vitro* cell-based binding and blocking activities (online supplemental figure 4A,B), even though Atezolizumab possesses almost twice the area at the interface (~1646Å^2 by PISA). Comparison of HZ-C-Ye-18 with another PD-L1 vHH termed KN035 (PDB: 5JDS)[32] shows that both these molecules contact with several PD-1 interaction sites on PD-L1, including I54, Y56, M115 and A121 (online supplemental figure 5B,C).

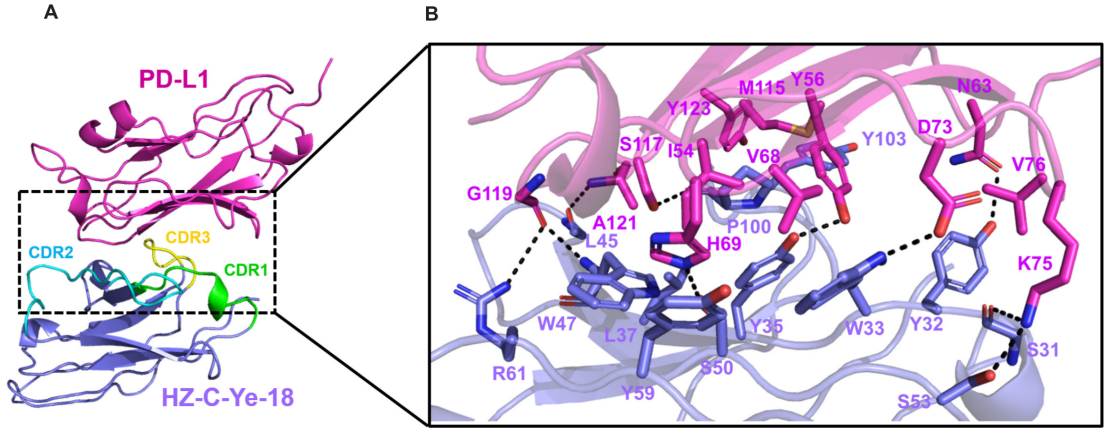

Figure 3 Detailed interaction sites between PD-L1 and HZ-C-Ye-18. (A) Overall structure of the PD-L1:HZ-C-Ye-18 complex (PDB: 7CZD). PD-L1 is shown in magenta, while HZ-C-Ye-18 is shown in purple. The CDR1, CDR2 and CDR3 domains of HZ-C-Ye-18 are colored green, cyan and yellow, respectively. (B) The interactions between PD-L1 and HZ-C-Ye-18. Hydrogen bonds are shown as black dashed lines.

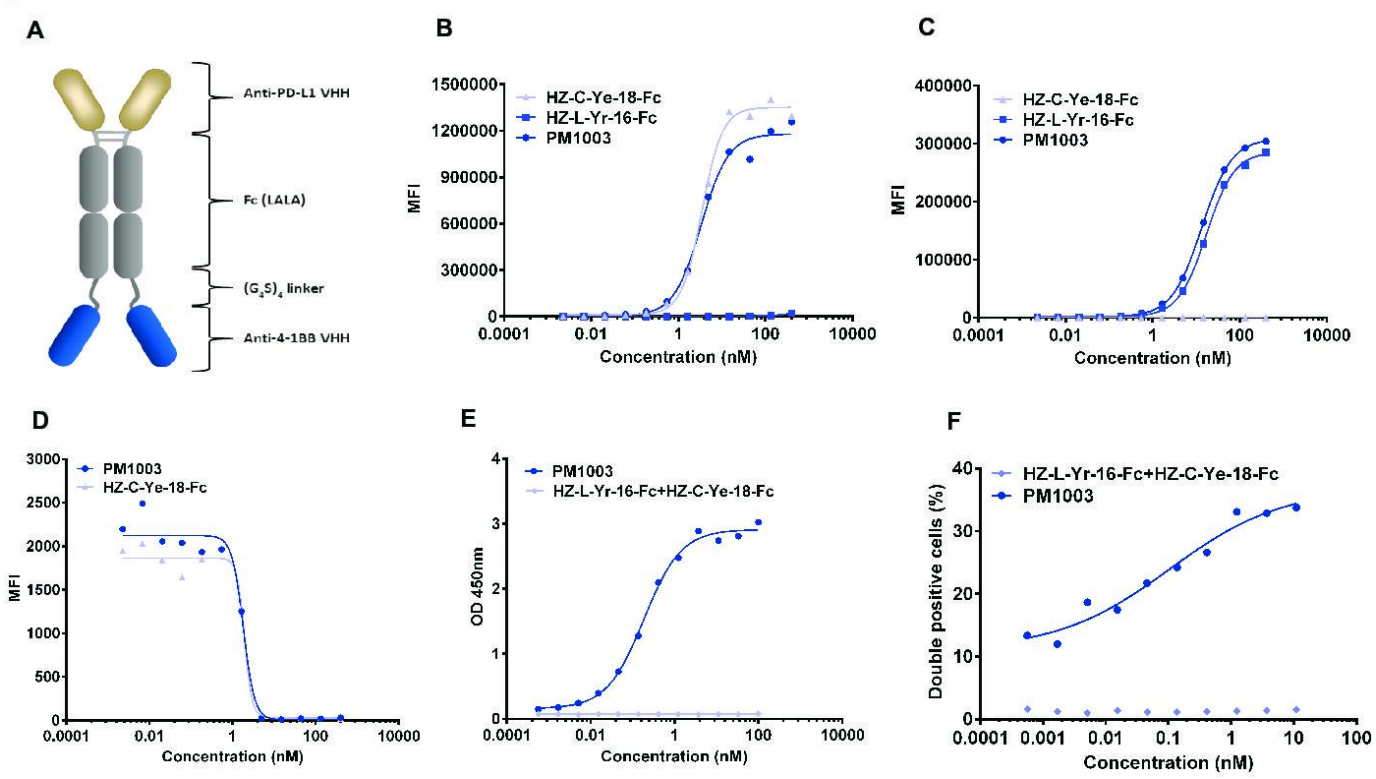

Figure 4 Structure of PM1003 and the binding activity of the bispecific antibody to both 4-1BB and PD-L1. (A) Structural representation of PM1003. (B) Binding of PM1003 to human PD-L1 overexpressed on CHO cells measured by flow cytometry. (C) Binding of PM1003 to human 4-1BB overexpressed on CHO cells measured by flow cytometry. (D) PM1003 blocks the interaction between PD-1/PD-L1 determined by flow cytometry. (E) PM1003 simultaneous binding to both human PD-L1 and human 4-1BB as determined by ELISA. (F) PM1003 simultaneous binding to both human PD-L1 and human 4-1BB overexpressing cells as determined by a cell bridging flow cytometry assay.

Design and characterization of an anti-PD-L1/4-1BB bispecific therapeutic

We proceeded to generate a bispecific molecule by fusing HZ-L-Yr-16 to the C terminus of HZ-C-Ye-18-Fc via a 20-residue-long linker (PM1003, figure 4A). The binding activity of each arm was similar to the parent antibodies in cell-based assays (figure 4B,C). Biolayer interferometry (BLI) analyses demonstrated high affinity binding to PD-L1 and 4-1BB (online supplemental figure 6A,B). More importantly, PM1003 did not show any non-specific binding to non-transfected CHO cells (online supplemental figure 6C) or 293F cells (online supplemental figure 6D). Functional assays showed that PM1003 efficiently inhibited PD-L1 binding to PD-1 on CHO-huPD-1 cells (figure 4D). The ability of PM1003 to facilitate co-binding of PD-L1 and 4-1BB was also evaluated by both BLI (online supplemental figure 6E) and ELISA (figure 4E). To evaluate if PM1003 facilitated cell bridging through simultaneously binding to both receptors, we fluorescently labeled CHO-huPD-L1 cells and CHO-hu4-1BB cells with different dyes and then treated them with PM1003 followed by flow cytometry analysis (online supplemental figure 6F). PM1003 induced the formation of doublets of CHO-huPD-L1 and CHO-hu4-1BB cells, while the combination of HZ-C-Ye-18-Fc and HZ-L-Yr-16-Fc did not (figure 4F).

PM1003-mediated T cell activation is dependent on crosslinking via PD-L1 cross-bridging

To demonstrate that PM1003 is an effective PD-L1-mediated 4-1BB agonist, Jurkat-4-1BB-NF-κB-Luc cells were cocultured with empty CHO or CHO-huPD-L1 cells and OKT-3/PM1003, then tested for NF-kB signaling through detection of luciferase activity. Maximum activation/luciferase signals were detected upon co-culture with CHO-huPD-L1 cells and PM1003 (figure 5A). Similarly, human primary T cells were stimulated by plate-bound OKT-3 mAb, then co-cultured with CHO-huPD-L1 or empty CHO cells with serially diluted PM1003 or HZ-L-Yr-16-Fc. T cell activation induced by PM1003 was only observed upon co-incubation with CHO-huPD-L1 cells (figure 5B,C). These data indicate that PM1003-mediated T cell activation was dependent on crosslinking via PD-L1-mediated cross-bridging. The activity of PM1003 was tested via an MLR, which utilizes human primary T cells and moDC expressing endogenous levels of both targets. PM1003 showed stronger T cell activation than the combination of anti-PD-L1 and anti-4-1BB antibodies (figure 5D), whereas HZ-L-Yr-16-Fc alone did not elicit any activation showing that PD-L1-mediated cross-bridging is a major contributor for the agonist activity of PM1003.

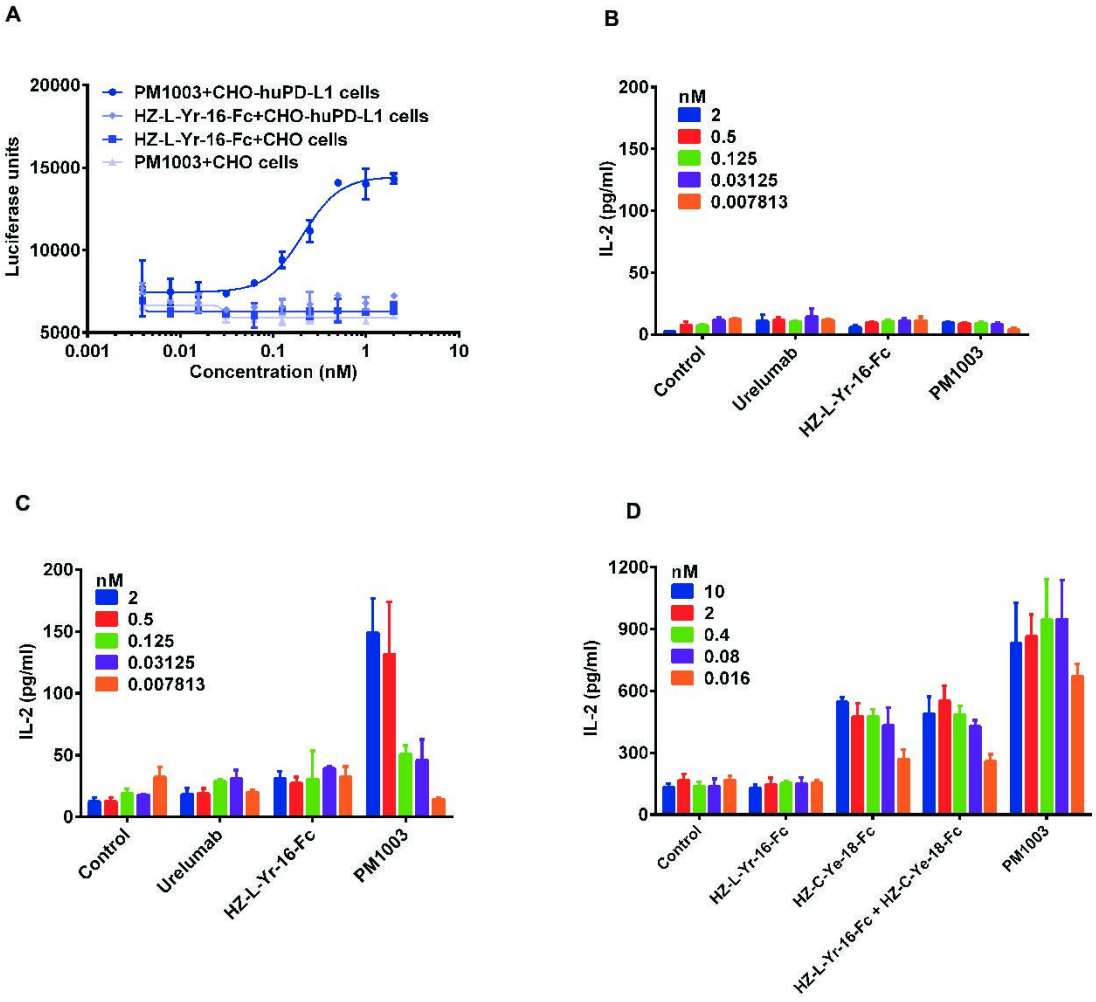

Figure 5 4-1BB agonism via PM1003 is dependent on crosslinking via PD-L1-mediated cross-bridging. (A) PM1003 activity of Jurkat-hu4-1BB-NF-κB luciferase cells incubated with CHO-huPD-L1 cells or PD-L1-negative CHO cells. (B) PM1003 activity in a human primary T cell activation assay with non-transfected CHO cells. (C) PM1003 activity in a human primary T cell activation assay with CHO-huPD-L1 cells. (D) PM1003 activity in a mixed lymphocyte reaction with monospecific components and in combination.

PM1003 suppresses tumor growth in syngeneic tumor models

To study the antitumor efficacy of PM1003 *in vivo*, CT-26-huPD-L1 cells and MC38-huPD-L1 cells were injected subcutaneously into the flank of human PD-1/PD-L1/4-1BB triple knock-in BALB/c mice and human PD-L1/4-1BB double knock-in C57BL/6 mice, respectively. In the CT-26-huPD-L1 tumor model, PM1003 was shown to substantially reduce tumor growth (figure 6A–C). Tumor inhibition was dose-dependent and significantly higher than that of the equimolar dose of Urelumab or the combination of the single agents. Dose-dependent antitumor efficacy was also observed in a MC38-huPD-L1 tumor model (figure 6D). In order to determine whether these complete responses (CRs) resulted in the induction of immune memory, mice with CRs were rechallenged with the same cell line in the inguinal mammary fat pad on the opposite flank. The inhibition of the 'rechallenged' tumor growth indicated that immune memory was induced in the PM1003-treated group (figure 6E).

PM1003 shows negligible hepatotoxicity

Since 4-1BB agonists have been shown to induce hepatotoxicity, we compared the toxicity profile of PM1003 with Urelumab in mice. Human 4-1BB knock-in mice were injected i.p. with PBS, Urelumab, or PM1003 every 5 days for four doses in total then euthanized 1 week later (figure 7A). Urelumab treatment induced a significant increase in liver and spleen weight, whereas PM1003 itself had no substantial effect (figure 7B,C). Serum levels of ALT increased on Urelumab treatment but not with PM1003 (figure 7D). Liver-infiltrating lymphocytes were also evaluated by H&E and CD8 IHC staining. Urelumab treatment induced significant levels of lymphocyte/$CD8^+$ T cell infiltration into liver tissues, whereas PM1003 did not (figure 7E–G). These results were consistent with the clinical toxicity profile of Urelumab. Collectively, PM1003 showed limited anti-4-1BB-mediated hepatotoxicity.

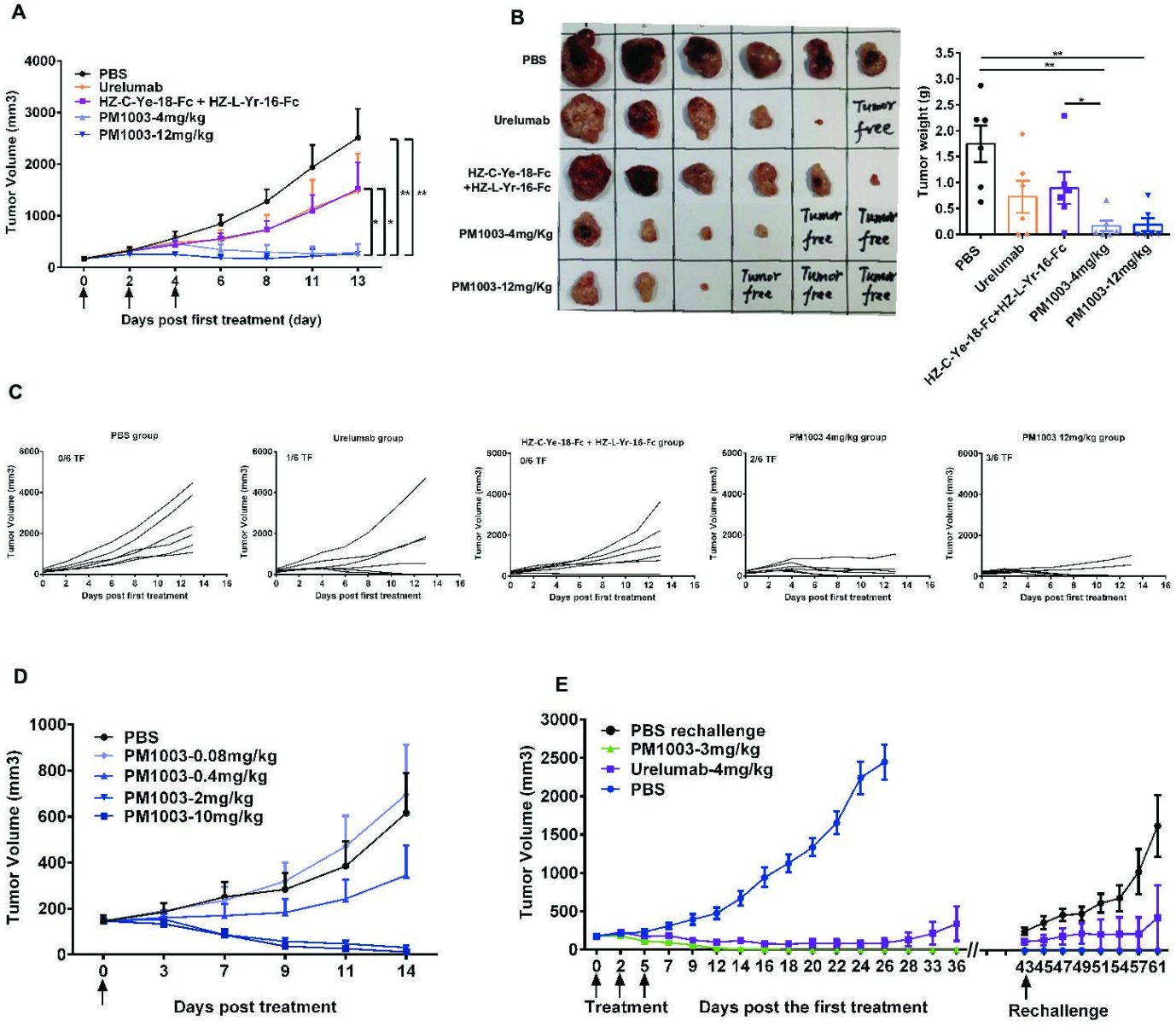

Figure 6 *In vivo* efficacy of PM1003 in CT-26-huPD-L1 and MC38-huPD-L1 mouse model. (A) Human PD-1/PD-L1/4-1BB triple knock-in mice were injected subcutaneously with 1×10^6 CT-26-huPD-L1 tumor cells, then molar equivalent doses of indicated antibodies were administrated on days 7, 9, 11. Tumor size was measured every other day. (B) Images of tumors (left) and tumor weight from mice (right). (C) Individual tumor growth spaghetti plots. Data are mean±SEM, *p<0.05, **p<0.01. (D) Dose-dependent efficacy and long-term immune memory induction of PM1003 were tested in a MC38-huPD-L1 mouse model. Human PD-L1/4-1BB double knock-in mice were injected subcutaneously with 1×10^6 MC-38-huPD-L1 tumor cells, then different doses of the indicated antibodies were administrated on days 7, 9, 11. Tumor size was measured every other day after the first treatment. (E) Tumor-free mice were re-challenged by injection of 1×10^6 MC-38-huPD-L1 tumor cells subcutaneously. Tumor size was measured every other day after the first treatment and on rechallenge.

DISCUSSION

We have discovered a novel single-domain antibody (HZ-L-Yr-16) with agonistic activity towards 4-1BB for the treatment of cancer. The differentiating traits of HZ-L-Yr-16 over its competitors ensures that desirable agonistic potency is facilitated with derisked on-target related liver toxicity—an issue that has hindered the clinical development of this class of therapeutic.[12 33–35] As such, HZ-L-Yr-16 is a valuable building-block for the engineering of 4-1BB-targeting multispecific therapeutics that may rely on tumor-specific crosslinking and cross-bridging between effector and tumor target cells.

HZ-L-Yr-16 binds to human and non-human primate 4-1BB strongly and specifically, targeting a novel binding epitope of 4-1BB at its CRD4 domain as determined by X-ray crystallography. This ensures that HZ-L-Yr-16 does not interfere with the natural interaction between 4-1BB and its ligand 4-1BBL. The binding epitope of HZ-L-Yr-16 is novel and unique compared with Urelumab and Utomilumab, which bind to CRD1 and between the CRD3 and

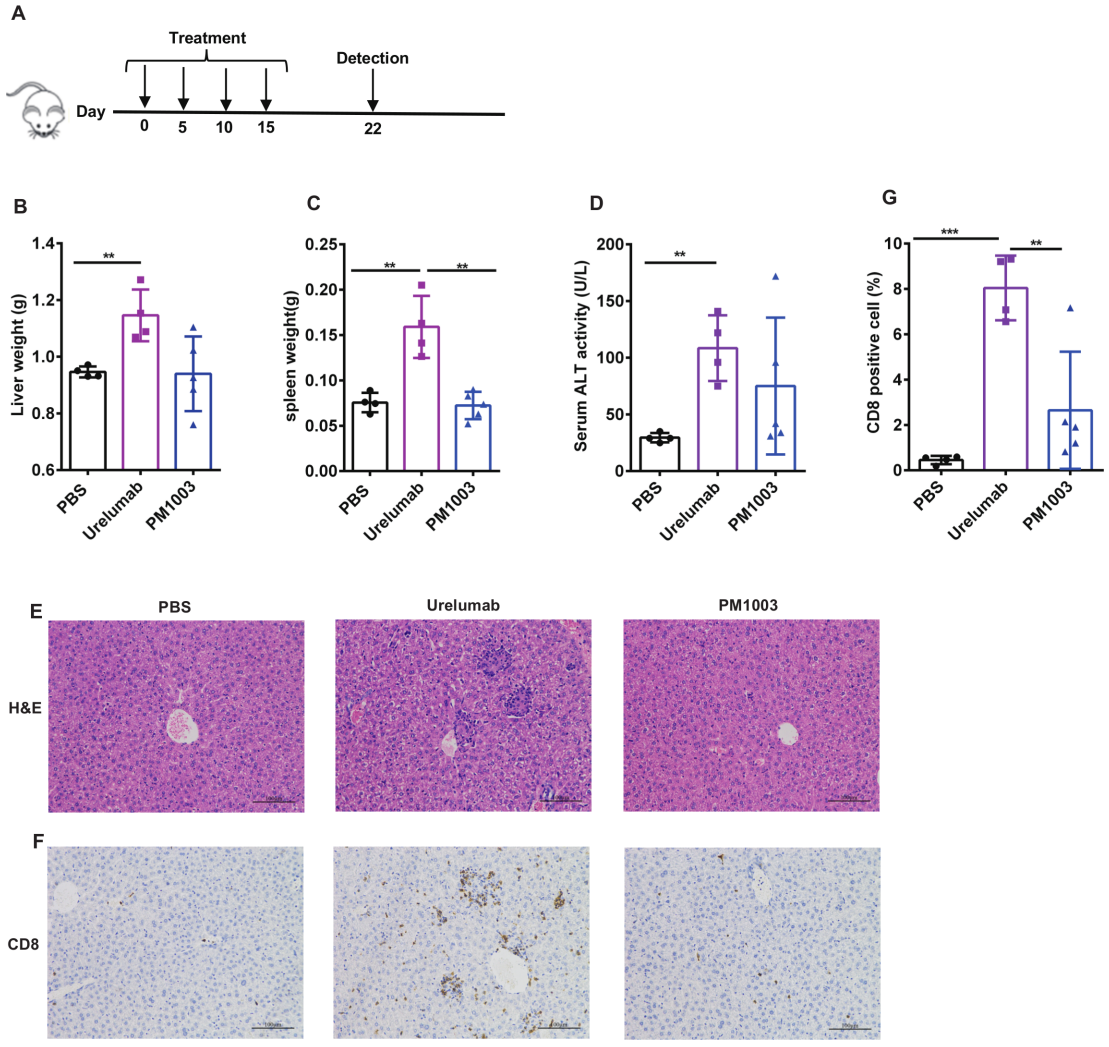

Figure 7 PM1003 was tested for liver pathology in a 4-1BB knock-in C57 mouse model. (A) Experimental protocol for the toxicity model. Human 4-1BB knock-in C57 mice (n=4 or 5/group) were treated with 10 mg/Kg Urelumab, 6.67 mg/Kg PM1003 or PBS on days 0, 5, 10 and 15. 7 days after the final treatment, (B) liver weight, (C) spleen weight, (D) serum ALT activity, (E) liver tissue HE staining, (F) liver tissue CD8-positive T cell IHC staining and (G) percentage of CD8-positive cell infiltration, were measured. Data are mean±SEM, **p<0.01, ***p<0.001.

CRD4 domains, respectively.[18] It has been suggested that the agonist activity of antibodies directed to the TNFR-superfamily members—as modeled on CD40—weakens from CRD1 to CRD4.[17] This suggests that the binding of agonist antibodies to more membrane proximal regions offer milder agonist activity. This could directly explain the vast differences in potency between Urelumab and Utomilumab, which have shown strong and weak agonist activity, respectively. HZ-L-Yr-16 binds to a unique epitope closer to the membrane proximal region compared with Urelumab and Utomilumab, providing some rationale for HZ-L-Yr-16 having a lowered risk of toxicity compared with Urelumab. To support this notion, we have shown that HZ-L-Yr-16 exhibits dose-dependent cross-bridging activity without activation of 4-1BB on primary T cells when added in solution. However, unlike Utomilumab, HZ-L-Yr-16 retains significant agonist activity.

It is unclear as to why Utomilumab binds to a more membrane-distal epitope as compared with HZ-L-Yr-16 but shows weak agonism activity and whether this lack of agonistic activity is connected to its ligand blocking ability. The alignment of our structure with ligand-bound 4-1BB (PDB: 6A3V) reveals the potential structural model for the ternary complex. Notably, as 4-1BB naturally exists as both monomers and dimers mediated by C121, how these associate with their ligand and agonist antibodies remain to be elucidated. The limited crosslinking of 4-1BB by 4-1BBL was proposed previously,[36] suggesting that the clustering of 4-1BB may occur in multiple modes. Structural analysis and modeling revealed the possibility for HZ-L-Yr-16 to bind either monomeric or dimeric 4-1BB molecules in the presence of its ligand (online supplemental figure 2D). Thus, HZ-L-Yr-16 and 4-1BBL might synergistically promote 4-1BB signaling during T cell activation. As mentioned, other studies have shown that the antibody binding epitope towards TNFR-superfamily members (CD40 and OX40) may determine agonistic strength. Agonist activity was observed to be stronger for

antibodies that bind to the membrane distal domain of CD40, but weaker for those binding to membrane distal domain of OX40.[17 37] Although we do not have access to a panel of antibodies that bind to every domain of 4-1BB, it is clear that different clones exhibit very distinct agonist profiles, and that the current evidence suggest that the binding to the distal N-terminal domain of 4-1BB may naturally offer a higher degree of agonist activity with potential toxicity issues (as with Urelumab). It is also understood that a fast association/dissociation (fast-on/fast-off) binding profile may improve the agonist activity of mAbs by offering a constant on/off binding flux. Thus, the strong binding strength and ligand blocking activities of Utomilumab might contribute to reduced activity.

To ensure that the toxicity related to 4-1BB agonists is restricted to the local tumor microenvironment, investigators have engineered bispecific molecules to bind to tumors with one arm and bridge over to 4-1BB receptors using the other.[19–22] This bridging effect between the effector and target cells ensures that 4-1BB is only activated in the presence of tumor cells. Here, we fused HZ-L-Yr-16 to the C-terminus of an anti-PD-L1 vHH that contains an effector-silenced human g1 Fc (HZ-C-Ye-18-Fc) resulting in the therapeutic candidate PM1003. HZ-C-Ye-18 is a potent blocker of the interaction between PD-1 and PD-L1 and through structural determination has an overlapping binding epitope similar to Atezolizumab. Both the PD-L1 and 4-1BB binding sites of PM1003 retain their potency in this bispecific form. Moreover, the bispecific antibody was shown to cross-bridge PD-L1- and 4-1BB-expressing cells and can bind to both antigens simultaneously at the protein level. These properties were reflected in cell-based activation assays using luciferase reporter cell lines and primary cells with and without PD-L1-expressing targets.

The synergy of combining both PD-L1 and 4-1BB binders in PM1003 was displayed in a tumor model where CT-26 cells with human PD-L1 knocked-in to replace the murine sequence were implanted into human PD-1/PD-L1/4-1BB triple knock-in mice. Our results show that PM1003 was much superior compared with the combination of anti-PD-L1+anti-4-1BB antibodies at medium (4 mg/kg) and high (12 mg/kg) doses. Dose-dependent antitumor efficacy was also confirmed in MC38-huPD-L1 knock-in cells implanted into human PD-L1/4-1BB double knock-in mice. PM1003 was also able to induce memory as shown in rechallenged mice. Finally, we showed that hepatotoxicity was kept at a minimum in mice treated with PM1003 compared with Urelumab, where liver weight, spleen weight and CD8+ T cell infiltration were significantly lower than the Urelumab group. Non-human primates are not a suitable model for evaluating the toxicity of Urelumab due to its known low to minimal cross-reactivity. As PM1003 has cross-reactivity to both cynomolgus PD-L1 and 4-1BB, we conducted a non-good laboratory practice (GLP) safety assessment in cynomolgus monkeys at 60 mg/kg without any signs of untoward toxicity (data in revision). These safety studies have helped to de-risk any potential toxicity issues before entering clinical trials.

There are a number of anti-PD-L1/4-1BB programs under development at present,[22] towards other tumor antigens/stromal markers, or using 4-1BBL instead of an antibody binder to activate 4-1BB.[20 38 39] Recently, RO7122290, an antibody targeting fibroblast activation protein (FAP), fused to 4-1BBL, was well-tolerated up to 2000 mg as a single-agent and 1000 mg in combination with atezolizumab, without reaching a maximum tolerated dose, showing the potential safety of this class of agent (DOI: https://doi.org/10.1016/j.annonc.2020.08.1145). From the current literature and information from the public domain, there is yet to be a fully characterized bispecific antibody that binds to the CRD4 domain of 4-1BB. We believe that this mild agonist activity is suitable for a PD-L1-based 4-1BB bispecific due to the high doses used for current anti-PD-L1 treatments. We also believe that PD-L1, which is upregulated after T cell activation and IFN-γ exposure, would provide a safer cross-bridging pair that is localized to the local tumor microenvironment.

CONCLUSION

PM1003 is a highly differentiating drug candidate that binds to a unique epitope on 4-1BB and facilitates receptor agonism with a lowered risk for toxicity issues. PM1003 has been shown to block potently the interaction between PD-1 and PD-L1 and to induce agonism towards 4-1BB only in the presence of PD-L1-mediated cross-bridging. Thus, PM1003 is a promising bispecific agent to be developed for the treatment of multiple solid tumors.

Author affiliations
[1]Shanghai Institute of Immunology, Department of Immunology and Microbiology, Shanghai Jiao Tong University School of Medicine, Shanghai, China
[2]Discovery Biology & Discovery Technology, Biotheus Inc, Zhuhai, China
[3]Discovery Biology, Biotheus (Suzhou) Co., Ltd, Suzhou, China
[4]Institutes of Biology and Medical Sciences, Soochow University, Suzhou, China

Acknowledgements We would like to thank the Biotheus Discovery Biology and Discovery Technology teams; Weihui Fu for the protein formulation study; Liping Wan for drug developability analysis; Xiaolin Liu and Yi Luo for scientific contribution and review; Tiantian Dong for preclinical assessment.

Contributors TZ and CW contributed equally. XM and YFX constructed the yeast display library and conducted the vHH selection. TW constructed the bispecific antibody and generated the protein material. TZ and SD designed and performed cell-based assays. CW, YH, YZ and WJ generated the materials for crystallization and determined the structures. ZY and TP designed and performed the BLI experiments. WH and SP performed the *in vivo* experiments. JS, XG, BL, AT and YDX provided guidance and support throughout. JZ, AT, BL and YDX assisted with manuscript revisions. TZ, CW, YFX, AT and XM generated figures and wrote the manuscript with input from all the authors.

Funding The authors have not declared a specific grant for this research from any funding agency in the public, commercial or not-for-profit sectors.

Competing interests The research was funded by Biotheus Inc. All authors are current employees of Biotheus. Inc, with the exception of JZ, TZ and BL who declare no competing interests.

Patient consent for publication Not required.

Provenance and peer review Not commissioned; externally peer reviewed.

Data availability statement Data are available in a public, open access repository. All data relevant to the study are included in the article or uploaded as supplementary information. Structural information and atomic coordinates have been deposited into the Protein Data Bank (PDB) with the accession codes 7CZD and 7D4B. Other data that support the findings of this study are available from the corresponding author upon request.

ORCID iD

Tianhang Zhai http://orcid.org/0000-0002-5285-5823

REFERENCES

1 Pardoll DM. Immunology beats cancer: a blueprint for successful translation. *Nat Immunol* 2012;13:1129–32.
2 Hodi FS, O'Day SJ, McDermott DF, *et al*. Improved survival with ipilimumab in patients with metastatic melanoma. *N Engl J Med Overseas Ed* 2010;363:711–23.
3 Robert C, Thomas L, Bondarenko I, *et al*. Ipilimumab plus dacarbazine for previously untreated metastatic melanoma. *N Engl J Med* 2011;364:2517–26.
4 Topalian SL, Hodi FS, Brahmer JR, *et al*. Safety, activity, and immune correlates of Anti–PD-1 antibody in cancer. *N Engl J Med* 2012;366:2443–54.
5 Hamid O, Robert C, Daud A, *et al*. Safety and tumor responses with lambrolizumab (Anti–PD-1) in melanoma. *N Engl J Med* 2013;369:134–44.
6 Wolchok JD, Kluger H, Callahan MK, *et al*. Nivolumab plus ipilimumab in advanced melanoma. *N Engl J Med* 2013;369:122–33.
7 Mahoney KM, Atkins MB. Prognostic and predictive markers for the new immunotherapies. *Oncology* 2014;28 Suppl 3:39–48.
8 Alexandrov LB, Nik-Zainal S, Wedge DC, *et al*. Signatures of mutational processes in human cancer. *Nature* 2013;500:415–21.
9 Le DT, Uram JN, Wang H, *et al*. Pd-1 blockade in tumors with mismatch-repair deficiency. *N Engl J Med Overseas Ed* 2015;372:2509–20.
10 Schaer DA, Hirschhorn-Cymerman D, Wolchok JD. Targeting tumor-necrosis factor receptor pathways for tumor immunotherapy. *J Immunother Cancer* 2014;2:7.
11 Chen S, Lee L-F, Fisher TS, *et al*. Combination of 4-1BB agonist and PD-1 antagonist promotes antitumor effector/memory CD8 T cells in a poorly immunogenic tumor model. *Cancer Immunol Res* 2015;3:149–60.
12 Segal NH, Logan TF, Hodi FS, *et al*. Results from an integrated safety analysis of Urelumab, an agonist Anti-CD137 monoclonal antibody. *Clin Cancer Res* 2017;23:1929–36.
13 Ho SK, Xu Z, Thakur A, *et al*. Epitope and Fc-mediated cross-linking, but not high affinity, are critical for antitumor activity of CD137 agonist antibody with reduced liver toxicity. *Mol Cancer Ther* 2020;19:1040–51.
14 Eskiocak U, Guzman W, Wolf B, *et al*. Differentiated agonistic antibody targeting CD137 eradicates large tumors without hepatotoxicity. *JCI Insight* 2020;5.
15 Kotanides H, Sattler RM, Lebron MB, *et al*. Characterization of 7A5: a human CD137 (4-1BB) receptor binding monoclonal antibody with differential agonist properties that promotes antitumor immunity. *Mol Cancer Ther* 2020;19:988–98.
16 Qi X, Li F, Wu Y, *et al*. Optimization of 4-1BB antibody for cancer immunotherapy by balancing agonistic strength with FcγR affinity. *Nat Commun* 2019;10:2141.
17 Yu X, Chan HTC, Orr CM, *et al*. Complex interplay between epitope specificity and isotype dictates the biological activity of anti-human CD40 antibodies. *Cancer Cell* 2018;33:664–75.
18 Chin SM, Kimberlin CR, Roe-Zurz Z, *et al*. Structure of the 4-1BB/4-1BBL complex and distinct binding and functional properties of utomilumab and urelumab. *Nat Commun* 2018;9:4679.
19 Compte M, Harwood SL, Muñoz IG, *et al*. A tumor-targeted trimeric 4-1BB-agonistic antibody induces potent anti-tumor immunity without systemic toxicity. *Nat Commun* 2018;9:4809.
20 Claus C, Ferrara C, Xu W, *et al*. Tumor-Targeted 4-1BB agonists for combination with T cell bispecific antibodies as off-the-shelf therapy. *Sci Transl Med* 2019;11:eaav5989.
21 Hinner MJ, Aiba RSB, Jaquin TJ, *et al*. Tumor-Localized costimulatory T-cell engagement by the 4-1BB/HER2 bispecific Antibody-Anticalin fusion PRS-343. *Clin Cancer Res* 2019;25:5878–89.
22 Lakins MA, Koers A, Giambalvo R, *et al*. FS222, a CD137/PD-L1 tetravalent bispecific antibody, exhibits low toxicity and antitumor activity in colorectal cancer models. *Clinical Cancer Research* 2020;26:4154–67.
23 Novarra S, Grinberg L, Rickert KW, *et al*. A hingeless Fc fusion system for site-specific cleavage by ides. *MAbs* 2016;8:1118–25.
24 Karplus PA, Diederichs K. Assessing and maximizing data quality in macromolecular crystallography. *Curr Opin Struct Biol* 2015;34:60–8.
25 McCoy AJ, Grosse-Kunstleve RW, Adams PD, *et al*. *Phaser* crystallographic software. *J Appl Crystallogr* 2007;40:658–74.
26 Murshudov GN, Vagin AA, Dodson EJ. Refinement of macromolecular structures by the maximum-likelihood method. *Acta Crystallogr D Biol Crystallogr* 1997;53:240–55.
27 Emsley P, Lohkamp B, Scott WG, *et al*. Features and development of *Coot*. *Acta Crystallogr D Biol Crystallogr* 2010;66:486–501.
28 Hezareh M, Hessell AJ, Jensen RC, *et al*. Effector function activities of a panel of mutants of a broadly neutralizing antibody against human immunodeficiency virus type 1. *J Virol* 2001;75:12161–8.
29 Bruhns P, Iannascoli B, England P, *et al*. Specificity and affinity of human Fcγ receptors and their polymorphic variants for human IgG subclasses. *Blood* 2009;113:3716–25.
30 Lee HT, Lee JY, Lim H, *et al*. Molecular mechanism of PD-1/PD-L1 blockade via anti-PD-L1 antibodies atezolizumab and durvalumab. *Sci Rep* 2017;7:5532.
31 Liu K, Tan S, Chai Y, *et al*. Structural basis of anti-PD-L1 monoclonal antibody avelumab for tumor therapy. *Cell Res* 2017;27:151–3.
32 Zhang F, Wei H, Wang X, *et al*. Structural basis of a novel PD-L1 nanobody for immune checkpoint blockade. *Cell Discovery* 2017;3:17004.
33 Bartkowiak T, Jaiswal AR, Ager CR, *et al*. Activation of 4-1BB on liver myeloid cells triggers hepatitis via an Interleukin-27–Dependent pathway. *Clin Cancer Res* 2018;24:1138–51.
34 Cheng L, Wang J, Li X, *et al*. Interleukin-6 induces Gr-1+CD11b+ myeloid cells to suppress CD8+ T cell-mediated liver injury in mice. *PLoS One* 2011;6:e17631.
35 Wang J, Zhao W, Cheng L, *et al*. CD137-mediated pathogenesis from chronic hepatitis to hepatocellular carcinoma in hepatitis B virus-transgenic mice. *J.i.* 2010;185:7654–62.
36 Li Y, Tan S, Zhang C, *et al*. Limited cross-linking of 4-1BB by 4-1BB ligand and the agonist monoclonal antibody Utomilumab. *Cell Rep* 2018;25:909–20.
37 Griffiths J, Hussain K, Smith HL, *et al*. Domain binding and isotype dictate the activity of anti-human OX40 antibodies. *Journal for ImmunoTherapy of Cancer* 2020;8:e001557.
38 Trüb M, Uhlenbrock F, Claus C, *et al*. Fibroblast activation protein-targeted-4-1BB ligand agonist amplifies effector functions of intratumoral T cells in human cancer. *J Immunother Cancer* 2020;8:e000238.
39 You G, Lee Y, Kang Y-W, *et al*. B7-H3×4-1BB bispecific antibody augments antitumor immunity by enhancing terminally differentiated CD8 $^{+}$ tumor-infiltrating lymphocytes. *Sci Adv* 2021;7:eaax3160.